Monte Carlo simulations of temperature programmed desorption spectra

B. Meng and W. H. Weinberg
Department of Chemical Engineering, University of California, Santa Barbara, California 93106-5080

(Received 17 May 1993; accepted 15 December 1993)

We introduce a Monte Carlo algorithm which simulates first-order temperature programmed desorption spectra using the correct connection between Monte Carlo simulation time and real time. The TPD spectra obtained from the Monte Carlo simulations are exactly the same as those calculated from the governing continuum differential equation for a noninteracting system. We discuss in some detail the effects of lateral interactions between adsorbates on the temperature programmed desorption spectra. We find that peak splitting of the temperature programmed desorption spectra characterizes an adsorbate configuration transition on the surface. Furthermore, we analyze in detail the behavior of the coverage-dependent activation energy and preexponential factor for the case of a repulsive nearest-neighbor interaction and find that kinetic compensation occurs in this case.

I. INTRODUCTION

Temperature programmed desorption (TPD) has been the most widely used experimental technique for the investigation of interactions between adsorbates and surfaces. The interpretation of TPD spectra has usually been carried out using the simple Arrhenius or Polanyi–Wigner expression for the rate coefficient, namely,

$$R_d = k_d^{(0)}(\theta)\exp(-E_d(\theta)/k_BT)\,\theta^n, \tag{1}$$

where R_d is the rate of desorption, $k_d^{(0)}(\theta)$ is the preexponential factor of the desorption rate coefficient, $E_d(\theta)$ is the activation energy of desorption, T is the temperature of the surface, θ is the fractional coverage of the adsorbate on the surface, and n is the order of the desorption reaction.[1–8] In the presence of adsorbate–adsorbate interactions, however, the activation energy and the preexponential factor may vary with the surface coverage of the adsorbate,[9] and the concentration term may not be so simple as θ^n.

Assuming localized adsorption (which does not preclude surface diffusion) on sites of specific symmetry (e.g., on top, twofold bridge, threefold, etc.), the kinetics of desorption can be described by a lattice-gas model. Although a simple expression can be constructed using the lattice-gas model, it cannot be solved exactly except in special cases.[10] Therefore, Bragg–Williams (mean-field),[11] Bethe–Peierls (quasi-chemical),[12–19] a combination of these two approximations,[20] and other analytical methods[21–28] have been introduced to take into account lateral interactions between the adsorbates. Since exact results of the lattice-gas model can be derived using Monte Carlo simulations (at least in principle), Monte Carlo simulations are now used extensively to study the kinetics of desorption.[29–44]

In this paper, we introduce a Monte Carlo algorithm to simulate TPD spectra with the correct connection between Monte Carlo simulation time and real time. Unlike Monte Carlo algorithms employed previously,[39–43] the time increment after a desorption event is calculated directly from the total desorption rate on the surface in our algorithm, and their relationship is derived simply from the rate equation. The algorithm provides a convenient way to study isosteric properties, where the surface coverage must be monitored. To demonstrate the methodology, we investigate first a noninteracting system. We then discuss the effects on the TPD spectra of nearest-neighbor and next-nearest-neighbor interactions between adsorbates as well as the geometry of the substrate. We also examine the behavior of the coverage-dependent activation energy and preexponential factor of desorption for the case of a repulsive nearest-neighbor interaction.

II. MODEL AND ALGORITHM

The catalytic surface is represented by either a square or a hexagonal lattice of adsorption sites. Monte Carlo simulations of the model have been conducted on $L\times L$ square or hexagonal lattices with periodic boundary conditions, where $L=40$ or 60 lattice constants. Here, we consider monomolecular (first-order) desorption, taking into account nearest-neighbor and next-nearest-neighbor interactions. Considering all the different types of local configurations of the adsorbate on the surface, the desorption rate equation has the form

$$\frac{-d\theta}{dt} = \sum_i \theta_i k_{d,i}^{(0)} \exp(-E_{d,i}/k_BT), \tag{2}$$

where $k_{d,i}^{(0)}$ is the preexponential factor of the desorption rate coefficient for molecules with local configuration of type i, θ_i is the fractional coverage of molecules with local configuration of type i, and $E_{d,i}$ is the activation energy of desorption for a molecule in a local configuration of type i, which is assumed to be given by

$$E_{d,i} = E_d(0) - N_{nn}(i)E_{nn} - N_{nnn}(i)E_{nnn}. \tag{3}$$

Here, $E_d(0)$ is the activation energy for desorption of an isolated admolecule. The quantities $N_{nn}(i)$ and $N_{nnn}(i)$ are the number of nearest neighbors and next-nearest neighbors of the desorbing molecule with a local configuration of type i, and E_{nn} and E_{nnn} are the nearest-neighbor and next-nearest-neighbor interaction energies. In the simulations, we assume that the preexponential factor of all local configurations is constant and equal to $k_d^{(0)}$.[45]

Equation (2) can also be written as

 0021-9606/94/100(7)/5280/10/$6.00

$$\frac{-dN}{dt} = \sum_i N_i k_d^{(0)} \exp(-E_{d,i}/k_B T), \tag{4}$$

where N_i is the number of molecules with local configuration of type i. Therefore, the time increment for desorption of a molecule from the surface is given by

$$\tau(N) = 1 \Big/ \sum_i N_i k_d^{(0)} \exp(-E_{d,i}/k_B T). \tag{5}$$

In evaluating the local configurations, we assume here that the rate of surface diffusion is much more rapid than that of desorption, i.e., the adsorbate is considered to be in a quasi-equilibrium state on the surface.[46] This assumption is frequently justified, because in most real systems involving adsorption on metallic surfaces the activation energy for surface diffusion is about 10%–15% of the molecule-surface bond energy. Hence, the Monte Carlo algorithm is formulated as follows:

(1) Randomly populate N_0 adsorbate molecules on the $L \times L$ lattice at an initial coverage of θ_0 $(=N_0/L^2)$.

(2) Relax the surface via surface diffusion until a thermodynamic equilibrium distribution of the adsorbate is established. This procedure is carried out as follows. An adsorbate molecule is chosen randomly, and then one of the z nearest-neighbor sites is also chosen randomly. If the site is occupied, the attempted hop fails, and the procedure is repeated. If the (jth) site is vacant, the particle hops into it from its original ith site with a probability $P_{i,j}(=\exp[-(E_j-E_i)/k_BT])$ if $E_j > E_i$, and with a probability of unity if $E_j < E_i$. The values of E_i and E_j are determined from Eq. (3). This procedure is repeated until an equilibrium distribution of the adsorbate on the surface is achieved.

(3) Calculate the desorption rate for each adsorbate molecule, k, via

$$r_k = k_d^{(0)} \exp(-E_k/k_B T). \tag{6}$$

The molecules that have the highest desorption rate, $r_{\max}$, are identified and updated throughout the course of the simulation.

(4) Choose an adsorbate molecule of index k at random and allow it to desorb with a probability of P_k $(=r_k/r_{\max})$. If a desorption event is realized, time is updated by an increment

$$\tau(N) = 1 \Big/ \sum_i N_i r_i, \tag{7}$$

which is the same as the mean interevent time derived from a collection of superposed Poisson events.[47] The temperature will also be updated after each desorption event by an increment $\beta\tau(N)$, where β is the heating rate of the experiment.

(5) Reestablish the surface in its new thermodynamic equilibrium distribution as in step 2 above.

(6) Repeat steps 3–5 until all molecules have desorbed.

The desorption rate in the time interval Δt is given by

$$R_d = \Delta N/\Delta t, \tag{8}$$

where ΔN is the number of adsorbate molecules which desorb in the time interval Δt.

TABLE I. Values of parameters used in the simulations. In all cases $k_d^{(0)}$ was taken to be 10^{13} s^{-1}, and, except where noted in the text, β was taken to be 5 K/s.

Set	Lattice	$E_d^{(0)}$ (kcal/mol)	E_{nn} (kcal/mol)	E_{nnn} (kcal/mol)
A	Hexagonal	31.6	2.20	0.00
B	Hexagonal	31.6	1.99	0.00
C	Hexagonal	31.6	2.94	0.00
D	Hexagonal	31.6	1.99	−0.39
E	Hexagonal	31.6	1.99	0.39
F	Square	30.6	2.00	0.00
G	Square	30.6	2.00	1.00

III. RESULTS AND DISCUSSION

In order to demonstrate this approach, we have simulated first an ideal case in which there are no lateral interactions. The TPD spectra employing the Monte Carlo simulations have been verified to be exactly the same as those calculated using the governing continuum differential equation[1] for all initial coverages.

We have also investigated the effect of lateral interactions on TPD spectra using the various parameter sets A–G of Table I. Figure 1 shows the TPD spectra simulated using parameter set A in Table I in which there is a repulsive nearest-neighbor interaction of strength $E_{nn}=2.20$ kcal/mol on a hexagonal lattice. As may be seen in Fig. 1, the nearest-neighbor repulsions result in a downshift of the peak temperature from 510 K to approximately 490 K as the initial surface coverage increases from $\theta_0=0.10$ to 0.33. The nearest-neighbor repulsions also cause the appearance of a second peak in the desorption spectra at a temperature of about 410 K for initial adsorbate coverages greater than 0.33. The high-temperature peak intensity and peak position do not vary for initial coverages greater than 0.33. As the surface coverage increases above 0.33, the intensity of the low-temperature peak increases, and its peak position shifts to slightly lower temperature. In Fig. 2, we show typical configurations of different adsorbate coverages that are obtained from the simulations. These snapshots show that a $(\sqrt{3} \times \sqrt{3})$R30° superstructure (with one admolecule and two vacancies per unit cell) grows in and reaches its maximum intensity at $\theta \approx 0.33$. For this perfect superstructure each admolecule has no nearest neighbors and six next-nearest neighbors. Domains of this superstructure may be seen in Fig. 2(b). Figure 2(a) reveals that there are very few nearest-neighbor admolecules on the surface, and this explains why the peak temperature corresponding to this coverage in Fig. 1 is essentially the same as the peak temperature found for the noninteracting case. As the surface coverage increases above 0.33, a $(\sqrt{3}\times\sqrt{3})$*R30° superstructure develops which contains two admolecules and one vacancy per unit cell. Rather large domains of this superstructure are apparent in Fig. 2(d).

Figure 3 shows the surface coverage of the adsorbate as a function of temperature for the six different initial surface coverages of Fig. 1. This figure shows clearly that for initial coverages $\theta_0 > 0.33$, the low-temperature peak and the high-temperature peak separate at the point where the adsorbate coverage is about 0.33. A comparison of Figs. 1–3 reveals

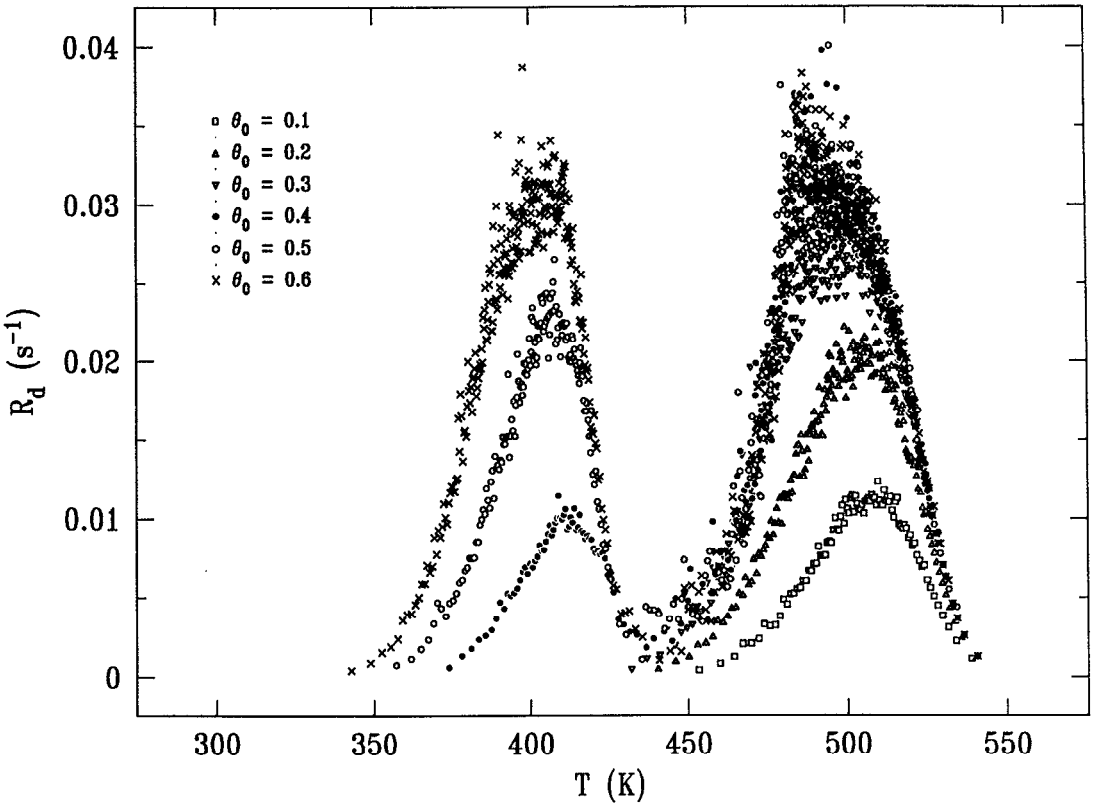

FIG. 1. TPD spectra generated by Monte Carlo simulations, using parameter set A in Table I, on a (60×60) hexagonal lattice for the indicated initial coverages.

that the high-temperature peak is associated with desorption from the phase in which the local coverage is at most 1/3, which corresponds to the $(\sqrt{3}\times\sqrt{3})$R30° superstructure that is formed because of nearest-neighbor repulsions. The low-temperature peak, on the other hand, is associated with desorption from the phase in which the local coverage is 2/3, the $(\sqrt{3}\times\sqrt{3})$*R30° superstructure, which has three nearest-neighbor repulsive interactions, cf. Fig. 2(d). Since there are nearest-neighbor repulsions, desorption is most likely to occur from the center of compact clusters in which the adsorbate has a maximum number of occupied nearest-neighbor sites, cf. Fig. 2(c).

Using the Taylor–Weinberg method,[8] we have also calculated the activation energy and preexponential factor for thermal desorption spectra generated using parameter set A of Table I. The initial coverage is held fixed at 0.5, and the heating rate is varied from 0.5 to 50 K/s. From this isosteric analysis the activation energy is given by

$$E_d(\theta) = -[\partial \ln(R_d/\theta)/\partial(k_B T)^{-1}]_\theta, \tag{9}$$

and the preexponential factor is given by

$$k_d^{(0)}(\theta) = \lim_{T\to\infty} R_d/\theta. \tag{10}$$

The calculated values of E_d and $k_d^{(0)}$ as a function of fractional surface coverage are shown in Figs. 4 and 5, respectively. For fractional coverages below about 0.2, E_d has the approximately constant value of 31.6 kcal/mol, while $k_d^{(0)}$ is also approximately constant with a magnitude of 10^{13} s^{-1}. Note that these are precisely the values of E_d and $k_d^{(0)}$ that were input into the simulation for the desorption of isolated admolecules. At fractional coverages approaching 0.5, E_d is approximately equal to 25 kcal/mol and $k_d^{(0)}$ is once again approaching 10^{13} s^{-1}. At intermediate coverages E_d goes through a maximum at $\theta\approx 0.3$ and then decreases precipitously to about 25 kcal/mol for $\theta\gtrsim 0.33$, cf. Fig. 4. Note that the apparent value of E_d *increases* by approximately 4 kcal/mol even though there are only *repulsive* interadsorbate interactions. Likewise, $k_d^{(0)}$ goes through a maximum at $\theta\approx$ 0.3 (which is more than two orders of magnitude greater than its zero-coverage value), decreases to about 10^{12} s^{-1} for $\theta\gtrsim 0.33$, and approaches 10^{13} s^{-1} at $\theta\approx 0.5$, cf. Fig. 5. This type of behavior has also been found using the variable order parameter, quasichemical approximation,[21] a four-site cluster approximation,[27] and the transfer-matrix technique,[23–26] and it bears strong qualitative similarities to the experimentally measured desorption of CO from Ru(001).[48–51]

The observations of Figs. 4 and 5 for $0.2<\theta<0.5$ are indicative of a chemical compensation effect, sometimes termed the Meyer–Neldel rule. As described in detail elsewhere for the case of a second-order surface reaction (31), this sympathetic variation in E_d and $k_d^{(0)}$ is due to a temperature dependence of the distribution of local configurations on the surface. Figures 4 and 5 now demonstrate that this effect can also be expected experimentally for first-order desorption. As may be seen in Figs. 2(a) and 2(b), desorption oc-

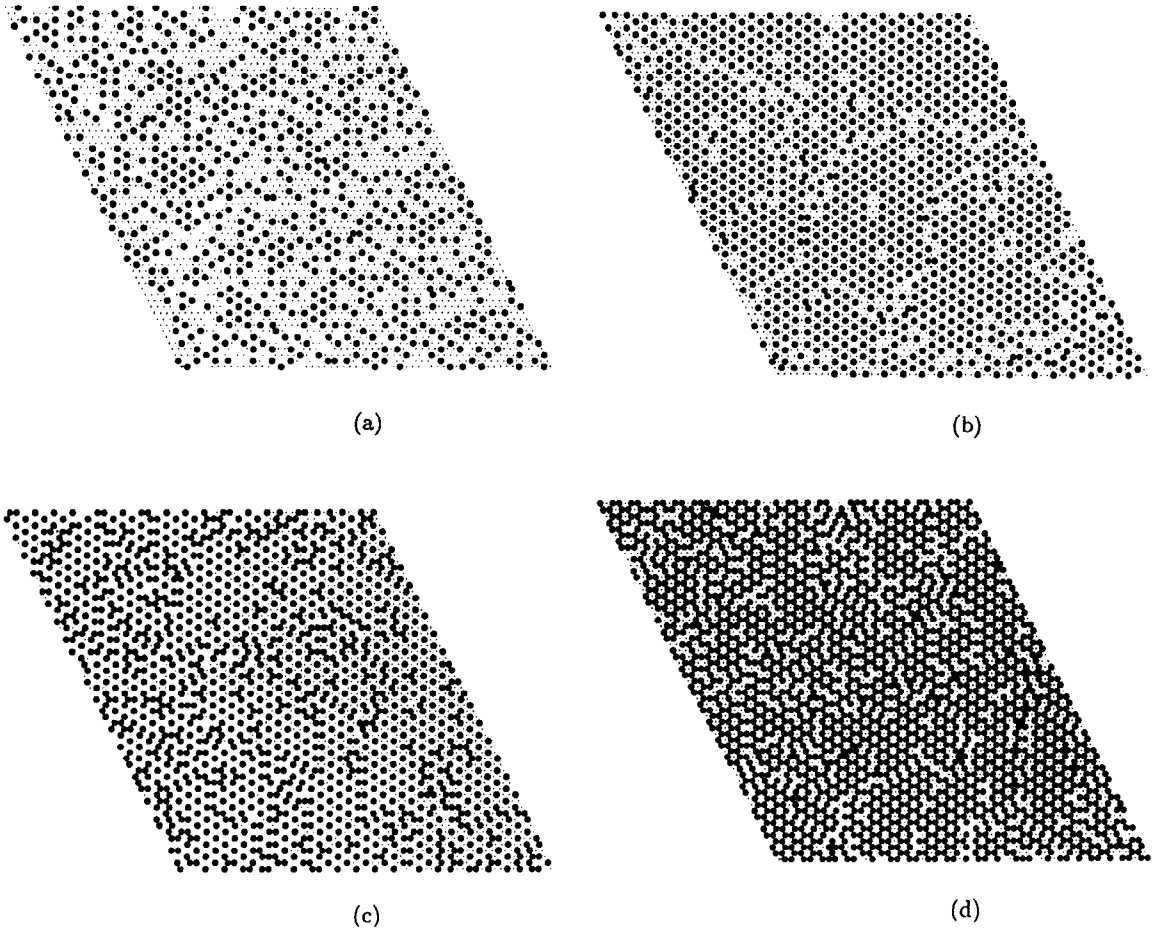

FIG. 2. Typical configurations of different initial coverages that are obtained from the simulations using parameter set A in Table I, where θ ranges from 0.2 to 0.6. The hexagonal lattice size is (60×60) for all these configurations. The dark circles represent adsorbate particles, and the smaller black dots represent lattice sites on the surface. These snapshots are taken when: (a) θ=0.2 and T=440 K, (b) θ=0.3 and T=430 K, (c) θ=0.4 and T=370 K, and (d) θ=0.6 and T=340 K.

curs mainly via isolated admolecules, which is completely consistent with Figs. 4 and 5. The precipitous drop in E_d near a fractional coverage of one-third is due to nearest-neighbor repulsions, cf. Fig. 2(c). At a coverage on the order of 0.5, desorption is predominantly from a (uniform) distribution of molecules with three nearest-neighbor repulsions, as manifested by $E_d \approx 25$ kcal/mol and $k_d^{(0)} \approx 10^{13}$ s^{-1}. At intermediate coverages the compensation effect results in the measurement of *apparent* rate parameters for desorption.

Simulations were also performed with different values of the nearest-neighbor interaction energy to quantify the fact that peak splitting in TPD is a consequence of the nearest-neighbor repulsions. Results of simulations with a less repulsive nearest-neighbor interaction, $E_{nn}=1.99$ kcal/mol (parameter set B in Table I) show that the high-temperature peak is essentially invariant compared to Fig. 1, whereas the low-temperature peak shifts up from 410 to 420 K compared with the spectra in Fig. 1, where $E_{nn}=2.20$ kcal/mol. This upshift is due to the effect of the nearest-neighbor repulsions, the strength of which has been reduced by 0.63 kcal/mol, i.e., 3(2.20–1.99). For TPD spectra employing a greater repulsive nearest-neighbor interaction, $E_{nn}=2.94$ kcal/mol (parameter set C in Table I), as would be expected, the high-temperature peak does not shift relative to the simulated TPD spectra of Fig. 1. As would also be expected, the low-temperature peak downshifts to approximately 370 K, which is completely consistent with three nearest-neighbor repulsions in the $(\sqrt{3}\times\sqrt{3})$*R30° superstructure with this stronger strength of repulsion. For an initial coverage greater than 0.66, there is an additional lower temperature desorption peak in the simulated TPD spectra. When one additional admolecule is added to the $(\sqrt{3}\times\sqrt{3})$*R30° superstructure, its local fractional coverage will be unity and it will experience six nearest-neighbor repulsions. The observed desorption temperature of approximately 250 K is completely consistent with six nearest-neighbor repulsions, the strength of each one of which is given by 2.94 kcal/mol. The three peaks in a simulated TPD spectrum corresponding to $\theta_0=0.8$ correspond predominantly to molecules that desorb with six nearest-neighbor repulsions, three nearest-neighbor repulsions, and no nearest-neighbor repulsions.

We have also investigated the effect of next-nearest-neighbor interactions on the simulated thermal desorption spectra. For TPD spectra simulated with a repulsive nearest-neighbor interaction, $E_{nn}=1.99$ kcal/mol, and an attractive next-nearest-neighbor interaction, $E_{nnn}=-0.39$ kcal/mol

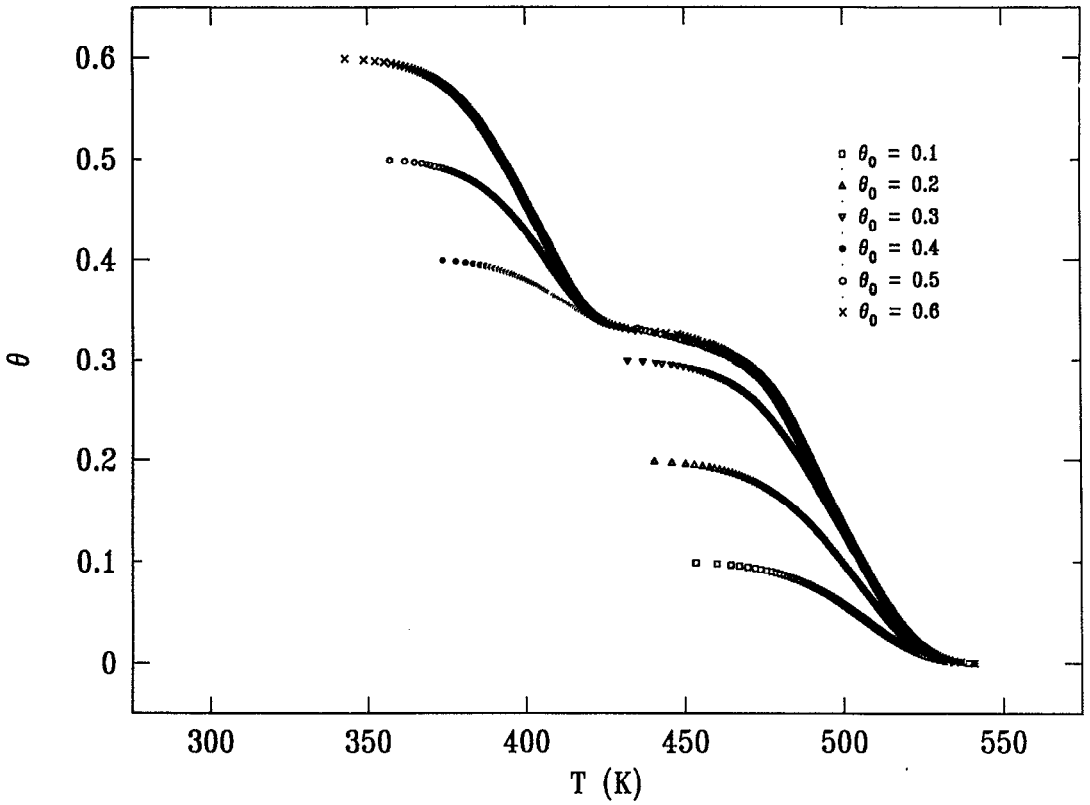

FIG. 3. The fractional coverage of adsorbate as a function of temperature for various initial coverages. These results are generated by Monte Carlo simulations on a (60×60) hexagonal lattice using parameter set A in Table I.

(parameter set D in Table I), the attractive next-nearest-neighbor interactions cause the spectra to become more narrow and to upshift their peak temperatures compared to the TPD spectra of Fig. 1. The distribution of local configurations is sharpened by the attractive interaction, as would be expected.[31] The leading edge of the low-temperature peak corresponds to admolecules with six next-nearest-neighbor attractions and three nearest-neighbor repulsions. The high-temperature peak corresponds largely to admolecules with no nearest-neighbor repulsions and a decreasing number of next-nearest-neighbor attractions. This effect of lateral interactions on the observed desorption peak temperature agrees qualitatively with the results of Lutsevich, Tkachenko, and Zhdanov[42] but disagrees with the results of Nagai and Bennemann[44] who found no upshift in desorption peak temperature when attractive next-nearest-neighbor interactions were included.

Adding repulsive next-nearest-neighbor interactions to

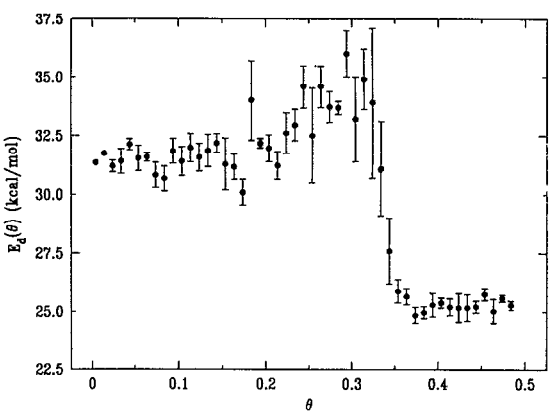

FIG. 4. Activation energy of desorption as a function of coverage. These results are generated by Monte Carlo simulations on a (40×40) hexagonal lattice using parameter set A in Table I.

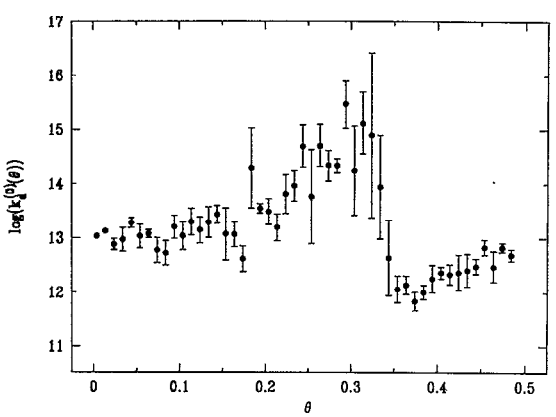

FIG. 5. Preexponential factor of desorption, in units of s^{-1}, as a function of coverage. These results are generated by Monte Carlo simulations on a (40×40) hexagonal lattice using parameter set A in Table I.

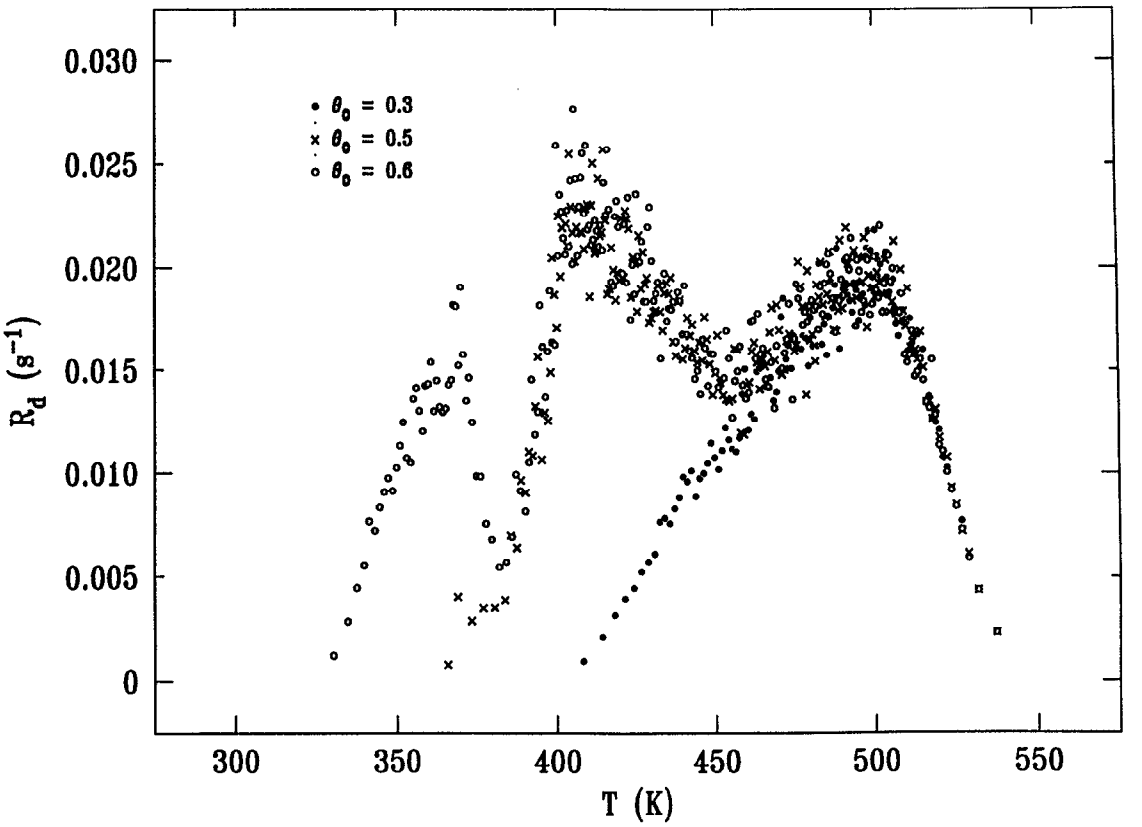

FIG. 6. TPD spectra generated by Monte Carlo simulations, using parameter set E in Table I, on a (40×40) hexagonal lattice for the indicated initial coverages.

repulsive nearest-neighbor interactions, on the other hand, results in the appearance of two broadened peaks for an initial surface coverage of 0.50 and three peaks for $\theta_0=0.60$. In Fig. 6 we show the simulated TPD spectra with a repulsive nearest-neighbor interaction, $E_{nn}=1.99$ kcal/mol, and a repulsive next-nearest-neighbor interaction, $E_{nnn}=0.39$ kcal/mol (parameter set E in Table I). For simulations with an initial coverage of 0.30, we obtain a broad desorption spectrum with a peak at about 500 K, cf. Fig. 6. For an initial surface coverage of 0.50, a second peak is observed just above 400 K. As the coverage decreases from 0.5 to approximately 0.2, the TPD spectrum coincides with that from $\theta_0=0.30$. For an initial coverage of 0.60, we observe three peaks in the simulated TPD spectrum of Fig. 6. The peak near 400 K overlaps with the one corresponding to $\theta_0=0.50$ when the surface coverage decreases from 0.60 to about 0.47, and the high-temperature peak overlaps with the one corresponding to $\theta_0=0.3$ when the surface coverage decreases to about 0.22, cf. Fig. 6. In Fig. 7, we show typical configurations at different coverages that are obtained from simulations on a (40×40) hexagonal lattice with parameters corresponding to the simulated TPD spectra of Fig. 6. Com-

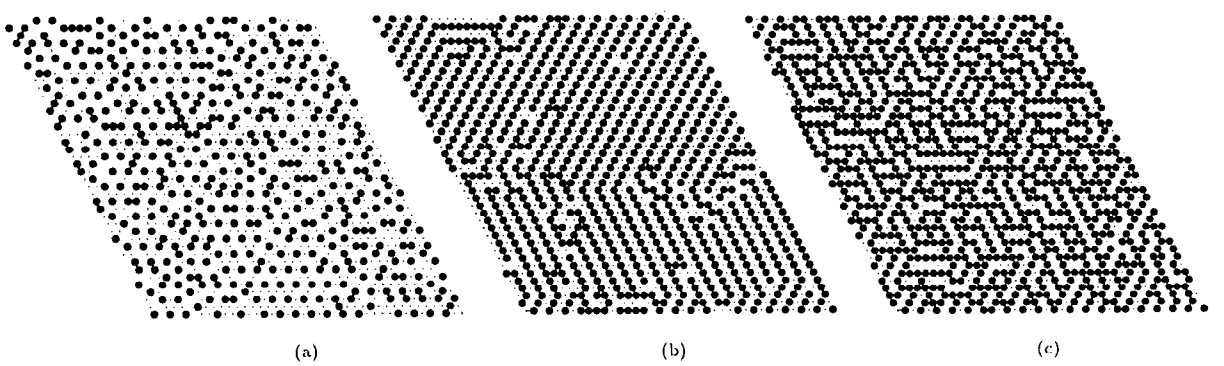

FIG. 7. Typical configurations of different initial coverages that are obtained from the simulations using parameter set E in Table I. The hexagonal lattice size is (40×40) for all these configurations. See Fig. 2. These snapshorts are taken when: (a) $\theta=0.30$ and T=405 K, (b) $\theta=0.50$ and T=365 K, and (c) $\theta=0.60$ and T=330 K.

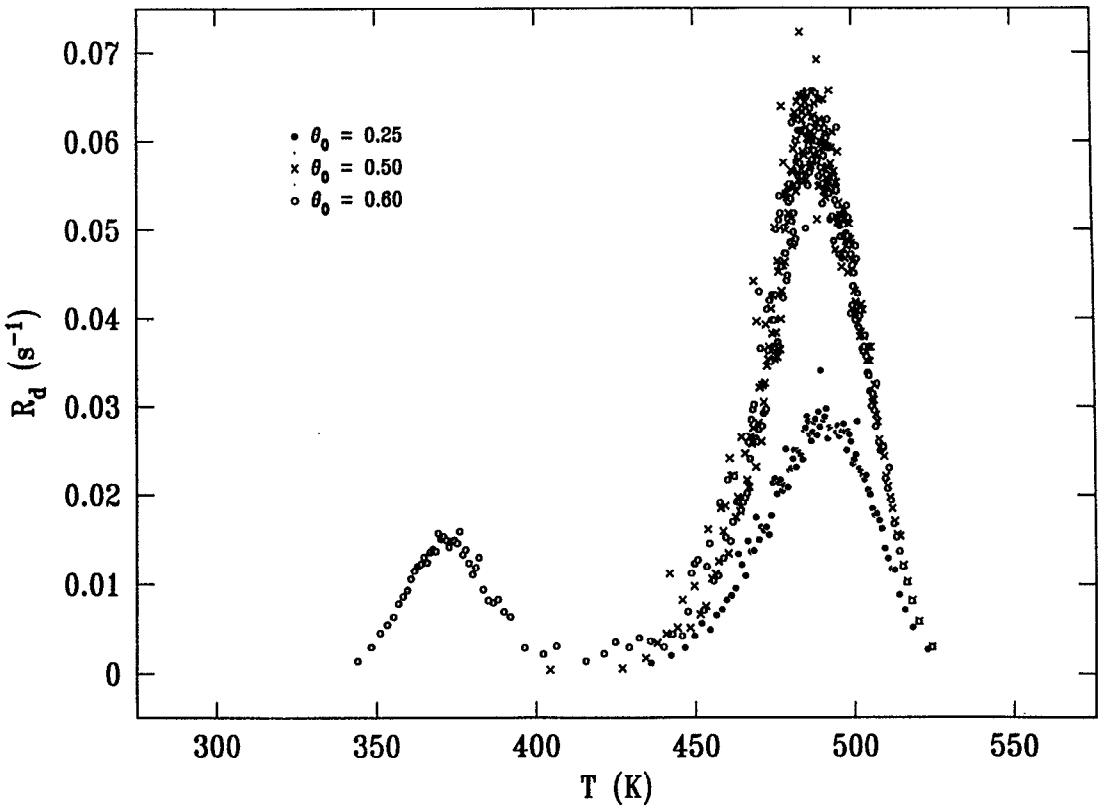

FIG. 8. TPD spectra generated by Monte Carlo simulations, using parameter set F in Table I, on a (40×40) square lattice for the indicated initial coverages.

paring Figs. 6 and 7 provides useful physical insight. The high-temperature peak above 450 K, for which $\theta \lesssim 0.25$, is associated with desorption from a weakly ordered (2×2) phase, cf. Fig. 7(a). The middle-temperature peak near 400 K, for which $\theta \lesssim 0.5$, is associated with desorption from a relatively well-ordered (1×2) phase, cf. Fig. 7(b), and the low-temperature peak near 370 K, for $0.5 < \theta < 0.6$, is associated with desorption from admolecules within small domains of (1×2) periodicity, cf. Fig. 7(c).

We have also conducted simulations on a square lattice in order to assess the effect of surface geometry on the TPD spectra. Figure 8 shows simulated TPD spectra using parameter set F in Table I, in which the repulsive nearest-neighbor interaction is $E_{nn} = 2.00$ kcal/mol, and there is no next-nearest-neighbor interaction. The repulsive nearest-neighbor interaction causes the TPD spectra for initial coverages greater than approximately 0.5 to split into two peaks at $\theta \approx 0.5$. Fig. 9 shows typical configurations for initial fractional coverages of 0.25, 0.5, and 0.6 that are obtained from the simulations. These snapshots show that local domains of poor $c(2\times2)$ order are formed at surface coverages below 0.5 upon annealing to just below the temperature at which desorption begins, cf. Fig. 9(a). At a surface coverage of 0.5, essentially perfect $c(2\times2)$ order is observed, as may be seen in Fig. 9(b). For surface coverages above 0.5, molecules adsorb within the $c(2\times2)$ superstructure, cf. Fig. 9(c), and the *repulsive* interactions they experience give rise to the low-temperature peak in the simulated TPD spectrum of Fig. 8. The high-temperature peaks in Fig. 8, for which $\theta < 0.5$, are associated with desorption from a weakly ordered $c(2\times2)$ phase.

Adding repulsive next-nearest-neighbor interactions to the repulsive nearest-neighbor interactions results in the appearance of three peaks for surface coverages greater than 0.5, as observed also in the case the hexagonal lattice, cf. Figs. 6 and 10. Figure 10 shows simulated TPD spectra using a repulsive nearest-neighbor interaction, $E_{nn} = 2.00$ kcal/mol, and a repulsive next-nearest-neighbor interaction, $E_{nnn} = 1.00$ kcal/mol (parameter set G in Table I). For simulations with an initial fractional coverage of 0.25, we obtain a spectrum with a single peak just below 500 K, similar to that which was observed in Fig. 8. Simulations with $\theta_0 = 0.5$ give rise to two peaks due to the next-nearest-neighbor repulsions. As the coverage decreases from 0.5 to about 0.2, the spectrum for $\theta_0 = 0.5$ coincides with that from $\theta_0 = 0.25$. For an initial fractional coverage of 0.6, we observe three peaks in Fig. 10. As the coverage decreases from 0.6 to about 0.45, the TPD spectra for $\theta_0 = 0.6$ and $\theta_0 = 0.5$ also become identical, cf. Fig. 10. In Fig. 11, we show typical configurations of the different annealed initial coverages that are obtained from the simulations. Comparing Figs. 10 and 11 reveals that the high-temperature desorption peak, for which $\theta < 0.25$, is associated with desorption from a weakly ordered (2×2) phase, cf. Fig. 11(a). The intermediate desorption peak near 425 K, for which $0.25 < \theta < 0.50$, is associated with desorption from a weakly ordered (1×2) phase, cf. Fig. 11(b), and the low-temperature peak for which $\theta > 0.50$ is associated with desorption from additional admol-

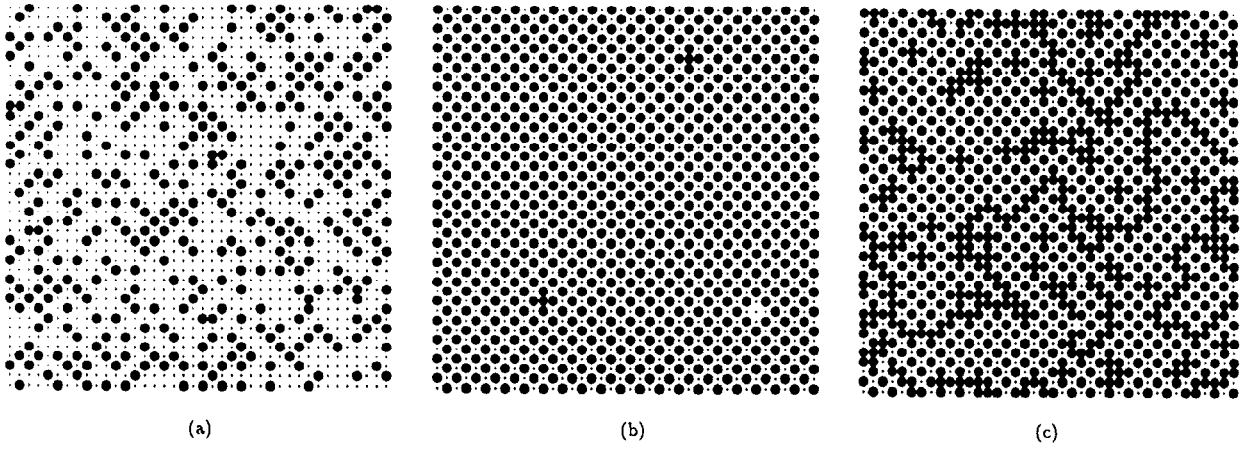

FIG. 9. Typical configurations of different coverages that are obtained from the simulations using parameter set F in Table I. The square lattice size is (40×40) for all these configurations. See Fig. 2. These snapshots are taken when: (a) θ=0.25 and T=435 K, (b) θ=0.50 and T=400 K, and (c) θ=0.60 and T =340 K.

ecules within the weakly ordered (1×2) phase.

Our results confirm and quantify the intuitive notion that multiple peaks in TPD spectra of interacting adsorbates are correlated with transitions in adsorbate configurations for ordered phases on the surface. Multiple peaks are usually separated from one another at coverages where the configuration (local or global) of the adsorbate transforms from one to another. The separation in temperature between the peaks is strongly dependent on the strength and nature of the lateral interactions. Larger repulsive interactions typically result in greater separation (and hence resolution) of the desorption peaks. Smaller repulsions result in less peak separation, and, possibly, single peak broadening rather than peak splitting. This is associated with weaker long-range order in the adphase. Attractive interactions result in a sharpening of the desorption peaks by virtue of a sharpening of the distribution of local configurations that exist on the surface.

The correlation of multiple peaks in TPD and surface

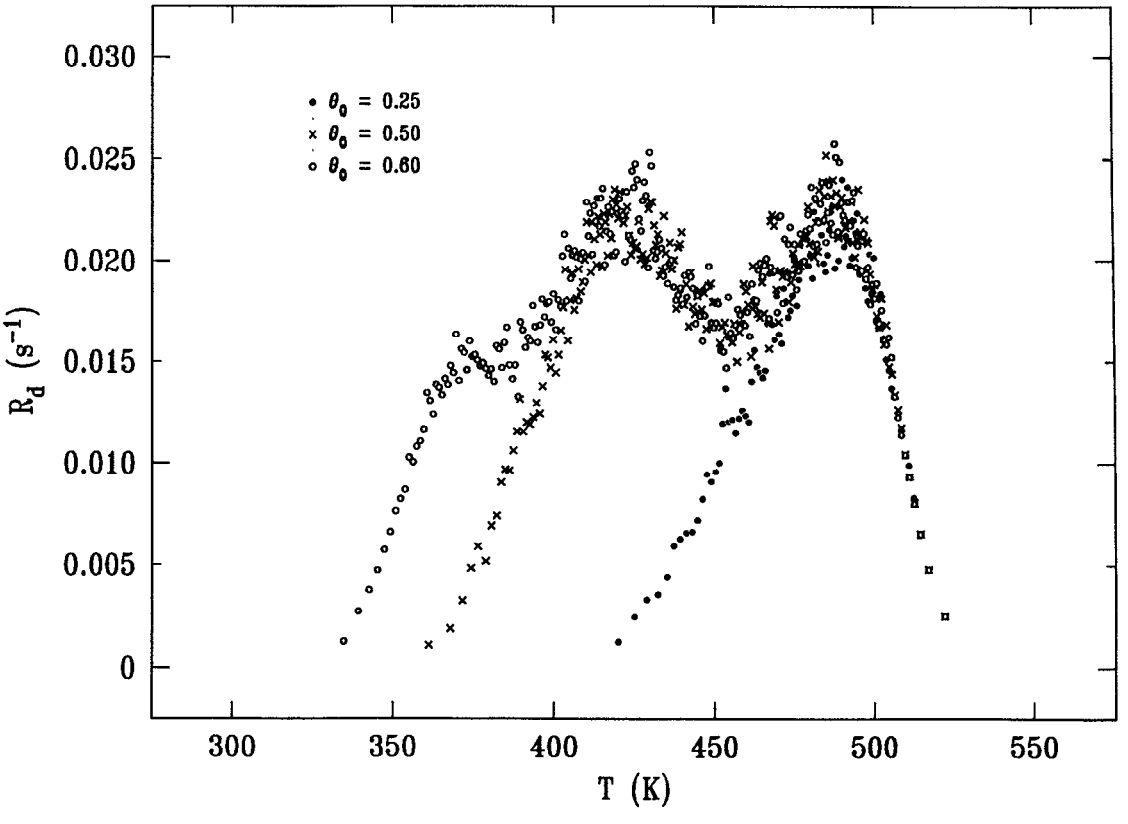

FIG. 10. TPD spectra generated by Monte Carlo simulations, using parameter set G in Table I, on a (40×40) square lattice for the indicated initial coverages.

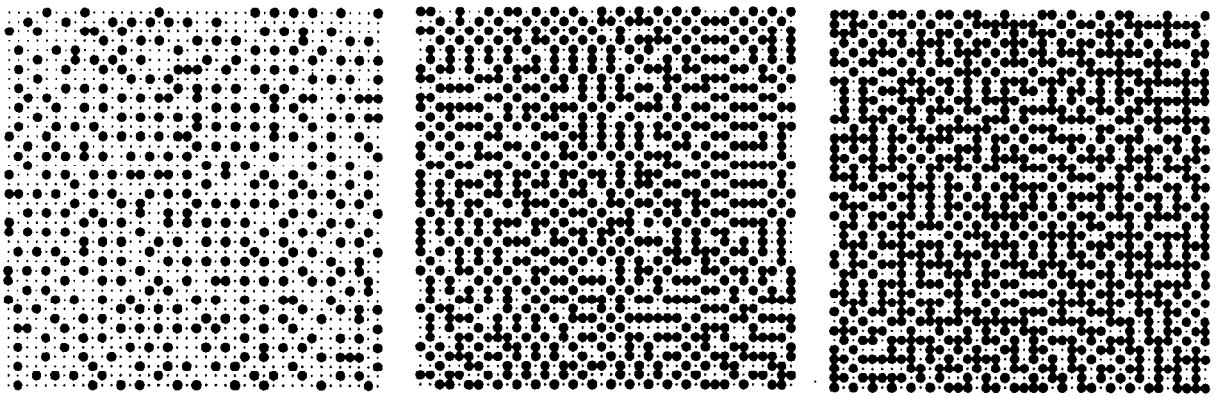

FIG. 11. Typical configurations of different initial coverages that are obtained from the simulations using parameter set G in Table I. The square lattice size is (40×40) for all these configurations. See Fig. 2. These snapshots are taken when: (a) θ=0.25 and T=415 K, (b) θ=0.50 and T=360 K, and (c) θ=0.60 and T=330 K.

phase transitions can also be understood by considering the time scale for desorption in the presence of lateral interactions. From Eq. (7) we see that τ(N) depends on the total surface coverage, the surface temperature, and the spacial distribution of the adsorbate molecules. Near the configuration transitions (or, more precisely, where the average local concentration changes), the spacial distribution of the adsorbate changes, and thus the time scale for desorption does as well. Hence, the TPD spectrum can exhibit multiple peaks.

IV. SYNOPSIS

We have introduced a Monte Carlo algorithm to simulate temperature programmed desorption spectroscopy, the notable features being the correct connection between Monte Carlo simulation time and real time, and the allowance for relaxation of the adlayer during the simulated desorption. We have demonstrated the validity of the algorithm by investigating overlayers without adsorbate–adsorbate interactions and showing that the simulated TPD spectra correspond to those calculated from the proper continuum master equation.

We have also found that the inclusion of nearest-neighbor repulsive interactions can lead to peak splitting for the cases of either no next-nearest-neighbor interactions, an attractive, or a repulsive next-nearest-neighbor interaction. Attractive next-nearest-neighbor interactions give rise to relatively sharper peaks in the simulated TPD spectra, whereas repulsive ones typically lead to peak broadening, an observation which can be understood in terms of the distribution of local surface configurations. We have also examined the coverage-dependent activation energy and preexponential factor for the case of a repulsive nearest-neighbor interaction, and we have found that the activation energy and preexponential factor vary sympathetically with coverage, and show a compensation effect. Finally, we have pointed out the connections among the observed peak splitting, the magnitude of the lateral interactions, and the occurrence of adsorbate configuration transitions in ordered phases.

ACKNOWLEDGMENT

We gratefully acknowledge the financial support of the National Science Foundation (Grant No. CHE-9300020).

[1] P. A. Redhead, Vacuum **12**, 203 (1962).
[2] A. M. de Jong and J. W. Niemantsverdriet, Surf. Sci. **233**, 355 (1990).
[3] E. Tronconi and L. Lietti, Surf. Sci. **199**, 43 (1988).
[4] D. A. King, T. E. Madey, and J. T. Yates, J. Chem. Phys. **55**, 3236 (1971).
[5] E. Bauer, H. Poppa, G. Todd, and F. Bonczek, J. Appl. Phys. **45**, 5164 (1974).
[6] J. L. Falconer and R. J. Madix, J. Catal. **48**, 262 (1977).
[7] C. M. Chan, R. Aris, and W. H. Weinberg, Appl. Surf. Sci. **1**, 360 (1978).
[8] J. L. Taylor and W. H. Weinberg, Surf. Sci. **78**, 259 (1978).
[9] V. P. Zhdanov, Surf. Sci. Rep. **12**, 183 (1991), and references therein.
[10] R. J. Baxter, *Exact Solved Models in Statistical Mechanics* (Academic, London, 1982).
[11] A. Córdoba and J. J. Luque, Phys. Rev. B **26**, 4028 (1982).
[12] V. P. Zhdanov, Surf. Sci. **102**, L35 (1981); **111**, L662 (1981); **123**, 106 (1983); **133**, 469 (1984); **137**, 515 (1986); **169**, 1 (1986); **179**, L57 (1987).
[13] B. Hellsing and V. P. Zhdanov, Chem. Phys. Lett. **147**, 613 (1988).
[14] H. J. Kreuzer and H. S. Payne, Surf. Sci. **198**, 235 (1988); **200**, L433 (1988); **205**, 153 (1988); **222**, 404 (1989).
[15] J. B. Benziger and G. R. Schoofs, J. Phys. Chem. **88**, 4439 (1984).
[16] S. Sundaresan and K. R. Kaza, Surf. Sci. **160**, 103 (1985); Chem. Eng. Commun. **32**, 333 (1985); **35**, 1 (1985).
[17] H. Asada and M. Masuda, Surf. Sci. **207**, 517 (1989).
[18] A. Surda and I. Karasova, Surf. Sci. **109**, 605 (1981).
[19] A. Surda, Surf. Sci. **220**, 295 (1989).
[20] J. L. Sales, G. Zgrablich, and V. P. Zhdanov, Surf. Sci. **209**, 208 (1989).
[21] H. Pak and J. W. Evans, Surf. Sci. **186**, 550 (1987).
[22] J. W. Evans, K. K. Hoffman, and H. Pak, Surf. Sci. **192**, 475 (1987).
[23] A. V. Myshlyavtsev and V. P. Zhdanov, Chem. Phys. Lett. **162**, 43 (1989).
[24] A. V. Myshlyavtsev, J. L. Sales, G. Zgrablich, and V. P. Zhdanov, J. Stat. Phys. **58**, 1029 (1990).
[25] S. H. Payne, H. J. Kreuzer, and L. D. Roelofs, Surf. Sci. Lett. **259**, L781 (1991).
[26] S. H. Payne, J. Zhang, and H. J. Kreuzer, Surf. Sci. **246**, 185 (1992).
[27] A. Wierzbicki and H. J. Kreuzer, Surf. Sci. **257**, 417 (1991).
[28] H. J. Kreuzer, Langmuir **8**, 774 (1992).
[29] E. S. Hood, B. H. Toby, and W. H. Weinberg, Phys. Rev. Lett. **55**, 2437 (1985).
[30] W. H. Weinberg, in *Kinetics of Interface Reactions*, Springer Series in Surface Science, Vol. 8, edited by M. Grunze and H. J. Kreuzer (Springer, Berlin, 1987), pp. 94–125.
[31] H. C. Kang, T. A. Jachimowski, and W. H. Weinberg, J. Chem. Phys. **93**, 1418 (1990).

[32] K. A. Fichthorn and W. H. Weinberg, Langmuir **7**, 2539 (1991).
[33] H. C. Kang and W. H. Weinberg, Acc. Chem. Res. **25**, 253 (1992).
[34] R. M. Lambert and M. E. Bridge, Proc. R. Soc. London **A370**, 545 (1980); Surf. Sci. **94**, 469 (1980).
[35] M. Silverberg and A. Ben-Shaul, Chem. Phys. Lett. **134**, 491 (1987); J. Chem. Phys. **87**, 3178 (1987); J. Stat. Phys. **52**, 1179 (1988); Surf. Sci. **214**, 17 (1989).
[36] M. Stiles and H. Metiu, Chem. Phys. Lett. **128**, 337 (1986).
[37] D. Gupta and C. S. Hirtzel, Chem. Phys. Lett. **149**, 527 (1988); Surf. Sci. **210**, 322 (1989); Mol. Phys. **68**, 583 (1989).
[38] J. W. Evans and H. Pak, Surf. Sci. **199**, 28 (1988).
[39] S. J. Lombardo and A. T. Bell, Surf. Sci. **206**, 101 (1988); **224**, 451 (1989); Surf. Sci. Rep. **13**, 1 (1991).
[40] J. L. Sales and G. Zgrablich, Surf. Sci. **187**, 1 (1987); Phys. Rev. **B35**, 9520 (1987).
[41] J. L. Sales, G. Zgrablich, and V. P. Zhdanov, Surf. Sci. **209**, 208 (1989).
[42] L. V. Lutsevich, O. A. Tkachenko, and V. P. Zhdanov, Langmuir **7**, 1225 (1991); **8**, 1757 (1992).
[43] J. M. Heras, A. P. Velasco, L. Viscido, and G. Zgrablich, Langmuir **7**, 1124 (1991).
[44] K. Nagai and K. H. Bennemann, Surf. Sci. **260**, 286 (1992).
[45] W. H. Weinberg, in *Dynamics of Gas-Surface Interactions*, edited by C. T. Rettner and M. N. R. Ashfold (Royal Society of Chemistry, Cambridge, 1991), pp. 171–220.
[46] D. Menzel, in *Kinetics of Interface Reactions*, Springer Series in Surface Science, Vol. 8, edited by M. Grunze and H. J. Kreuzer (Springer, Berlin, 1987), pp. 2–18.
[47] K. A. Fichthorn and W. H. Weinberg, J. Chem. Phys. **95**, 1090 (1991).
[48] H. Pfnür, P. Feulner, H. A. Engelhardt, and D. Menzel, Chem. Phys. Lett. **59**, 481 (1978).
[49] E. D. Williams and W. H. Weinberg, Surf. Sci. **82**, 93 (1979).
[50] E. D. Williams, W. H. Weinberg, and A. C. Sobrero, J. Chem. Phys. **76**, 1150 (1982).
[51] H. Pfnür, P. Feulner, and D. Menzel, J. Chem. Phys. **79**, 4613 (1983).